Chinese Chemical Letters 36 (2025) 110608

Contents lists available at ScienceDirect

Chinese Chemical Letters

journal homepage: www.elsevier.com/locate/cclet

Construction of sintering-resistant gold catalysts *via* ascorbic-acid inducing strong metal-support interactions

Yunxia Liu[a,b,c], Guandong Wu[a,b], Lin Li[a], Yiming Niu[d], Bingsen Zhang[d], Botao Qiao[a,*], Junhu Wang[a,b,*]

[a] CAS Key Laboratory of Science and Technology on Applied Catalysis, Dalian Institute of Chemical Physics, Chinese Academy of Sciences, Dalian 116023, China
[b] Mössbauer Effect Data Center, Dalian Institute of Chemical Physics, Chinese Academy of Sciences, Dalian 116023, China
[c] University of Chinese Academy of Sciences, Beijing 100049, China
[d] Shenyang National Laboratory for Materials Science, Institute of Metal Research, Chinese Academy of Sciences, Shenyang 110016, China

ARTICLE INFO

Article history:
Received 12 June 2024
Revised 14 October 2024
Accepted 3 November 2024
Available online 4 November 2024

Keywords:
Supported metal catalyst
Adsorbate
L-Ascorbic acid
Oxygen vacancy
Strong metal-support interaction

ABSTRACT

Maintaining high metal dispersion of supported metal catalysts to achieve superior reactivity under harsh conditions poses one of the main challenges for their practical applications. Constructing and regulating the strong metal-support interactions (SMSI) by diverse methodologies has emerged as one of the promising approaches to fabricating robust supported metal catalysts. In this study, we report an L-ascorbic acid (AA)-inducing strategy to generate SMSI on a titania-supported gold (Au) catalyst after high-temperature treatment in an inert atmosphere (600 °C, N_2). The AA-induced SMSI can efficiently stabilize Au nanoparticles (NPs) and preserve their catalytic performance. The detailed study reveals that the key to realizing this SMSI is the generation of oxygen vacancies within the TiO_2 support induced by the adsorbed AA, which drives the formation of the TiO_x permeable layer onto the Au NPs. The strategy could be extended to TiO_2-supported Au catalysts with different crystal phases and platinum group metals, such as Pt, Pd, and Rh. This work offers a promising novel route to design stable and efficient supported noble metal catalysts by constructing SMSI using simple reducing organic adsorbent.

Metal oxide supported noble metal catalysts play vital roles in heterogeneous catalysis due to their excellent catalytic activity and/or selectivity for diverse chemical transformations [1–3]. Metal oxide serving as a support can not only disperse and anchor active metal species but also interact with them in many ways, significantly influencing the catalytic performance [4–6]. Classical strong metal-support interaction (SMSI) is one of the most important metal-support interactions which was first discovered by Tauster *et al.* [7] to describe the decrease or loss of chemisorption abilities toward small molecules (CO/H_2) of TiO_2-supported platinum group metal (PGM) NPs after high-temperature reduction treatment. One of the typical characteristics of the classical SMSI phenomenon is the reduced metal oxide support migrating onto the metal NPs surface to form an encapsulation structure [2,8–10]. Therefore, constructing overlayers of SMSI has been widely used to enhance the sinter resistance and high-temperature stability of the supported metal catalysts [11–13], especially for the metals with low Tammann temperature and the catalysts used in harsh operating conditions. However, this is often at the cost of activity loss due to the substantial crystalline overlayers, making it difficult for reactants to reach the active sites [14].

In recent years, numerous studies have focused on developing new routes to construct SMSI at milder conditions including wet-chemistry [15], ultrafast laser [16], ultrasonication [17] and mechanochemistry [18,19]. On the other hand, various adsorbed species induction, rather than the traditional thermally treatment in specific reductive gases (H_2/CO), can promote the metal catalysts reconstruction. This type SMSI named adsorbate-induced SMSI (A-SMSI) and with the amorphous encapsulation structure can ensure active metal sites remain accessible. For example, Christopher *et al.* [20] reported that HCO_x adsorbates can induce the formation of A-SMSI on TiO_2- and Nb_2O_5-supported Rh NPs at 150–300 °C. The generation of A-SMSI state changes the selectivity switch from CH_4 to CO in the CO_2-reduction process.

For a long time, it has been recognized that Au cannot form SMSI, because of its low work function and surface energy [21–23] compared with other noble metals and its low ability to dissociate molecular hydrogen. Until 2017, our group reported classic

* Corresponding authors.
E-mail addresses: bqiao@dicp.ac.cn (B. Qiao), wangjh@dicp.ac.cn (J. Wang).

https://doi.org/10.1016/j.cclet.2024.110608
1001-8417/

SMSI could be generated between Au and TiO_2 for the first time [24], which has been widely recognized for its excellent stability and unusually high catalytic performance [25]. Recently, we developed exogenous adsorption methods to construct SMSI in Au/PGMs supported on TiO_2, which also produced permeable overlayers by melamine induced and did not recede in the oxidation atmosphere [26,27]. This exogenous adsorption strategy induces A-SMSI and offers new opportunities for constructing sintering-resistant Au-based catalysts that exposed active sites maintain high activity and tunable reaction performance.

However, despite the extensive studies, the mechanisms of forming SMSI are still not fully understood up to now, and the widely accepted consensus is only a basic principle of minimizing the catalyst system surface energy as the underlying thermodynamic driving force. The electron transfer [28] induced support suboxide species migration on the metal NPs surface to generate encapsulation structure [21,29] and/or to form alloy [30,31] has also been proposed to explain the SMSI phenomenon. In addition, the formation of defects or vacancies in supports has also been considered a prerequisite in diverse catalyst systems for the occurrence of SMSI. For example, it was found that ultrafast laser excitation can induce SMSI of Pt/CeO_2 catalyst through forming surface defects and CeO_x migration [16], as well as mechanochemistry-driving approach was developed for SMSI construction [17,19]. A-SMSI can induce the formation of the permeable overlayers to ensure that the active sites are accessible. However, many cases of A-SMSI are formed under specific reaction conditions, which limits its further regulation and wide application. Therefore, it is still desired yet has room to develop new methods to construct SMSI, particularly those facile and universal for a wide range of catalyst systems, to synthesize high-performing catalysts and further understand the formation mechanism of SMSI.

In this work, we demonstrate that L-ascorbic acid (AA) modification followed by high-temperature treatment in inert atmosphere can construct SMSI in an Au/TiO_2 system. The permeable TiO_x overlayer and suppressed CO chemisorption confirms the formation of the SMSI, which not only inhibits the sintering of gold nanoparticles (NPs) but also allows the permeation of the reactant molecules. A detailed study revealed that the generation of oxygen vacancies in the TiO_2 support induced by AA adsorption contributes to activating the support surface, which is vital for the migration of TiO_x species to cover Au NPs. As a result, the catalysts with AA-induced SMSI showed remarkable catalytic activity and stability in the CO oxidation reaction. In addition, this facile and efficient strategy could be extended to TiO_2 support with other crystal phases (anatase and rutile) and TiO_2-supported PGMs (Pt, Pd, and Rh). This work develops a simple and universal approach to induce SMSI, providing a new route for the preparation of efficient and stable supported noble metal catalysts.

Au/TiO_2 catalyst was synthesized by a deposition-precipitation (DP) method with nominal 5 wt% Au loading on a commercial Degussa P25 support. Scheme 1 presents the illustration that the catalyst was modified by AA, followed by heat treatment at 600 °C in an N_2 atmosphere, denoted as Au/TiO_2@AA-N600. The actual Au loading of Au/TiO_2 determined by an inductively coupled plasma optical emission spectrometry (ICP-OES) was 2.4 wt% (Table S1 in Supporting information), much lower than the nominal one, suggesting serious metal loss during catalyst preparation, which is consistent with previous studies [32,33]. The X-ray diffraction (XRD) patterns of the as-prepared catalyst display intense peaks corresponding to the anatase (PDF #21-1272) and rutile (PDF #21-1276) phases, as shown in Fig. S1 (Supporting information). However, the characteristic diffraction peaks of Au, such as Au (111) at $2\theta = 38.2°$, are almost unobservable. The patterns of other Au catalysts (Au/TiO_2@AA, Au/TiO_2@AA-N600, and Au/TiO_2-N600) are similar to that of Au/TiO_2. Considering the relatively high Au loading (2.4 wt%), the result suggests a high dispersion of Au NPs on the support [34]. To further investigate the textural structure of the prepared Au nanocatalysts, the N_2 adsorption/desorption isotherms were collected at 77 K. As shown in Fig. S2 and Table S2 (Supporting information), all samples present similar type IV isotherms, indicating these catalysts have a mesoporous structure and the treatment process had no significant influence on their textural structure.

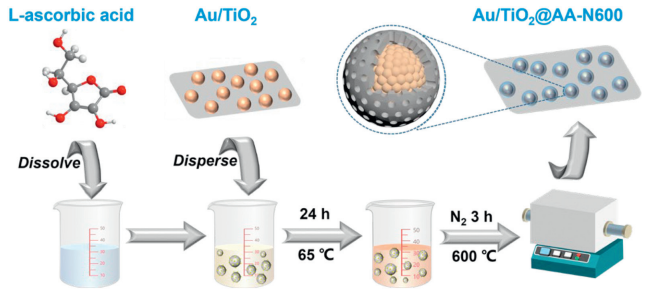

Scheme 1. Schematic illustration of the synthesis process. Synthesis of Au/TiO_2 by the deposition-precipitation (DP) method, through the dispersion of the Au/TiO_2 sample in L-ascorbic acid (AA) aqueous solution and treated in N_2 flow at 600 °C encapsulation of Au NPs within permeable TiO_x overlayer formation.

Transmission electron microscopy (TEM) was therefore employed to examine the size and high dispersion of Au NPs. High-resolution transmission electron microscopy (HRTEM) images of the series catalysts are shown in Fig. 1. Either the pristine Au/TiO_2 catalyst or the one after modification with the adsorbent AA shows the completely bare Au NPs with an average size of 2–3 nm (Figs. 1a, b, d, e, g, and h), demonstrating the lack of SMSI. The modification by AA has caused a slight increase in the average Au particle size (from 2.6 nm to 2.9 nm), which is likely due to an Ostwald ripening of the Au NPs in the AA solution. Interestingly, the surface of Au NPs of Au/TiO_2@AA-N600 samples is covered by a thin layer after heating treatment in N_2 at 600 °C (Fig. 1c), regardless of the particle size (Fig. S3 in Supporting information). It should be noted that with the modification of AA, such a high-temperature treatment only led to a slight sintering of Au NPs from 2.9 nm to an average size of 3.3 nm (Figs. 1f and i), suggesting an excellent sintering resistance. In contrast, the Au/TiO_2-N600 catalyst without AA modification directly treated in an inert atmosphere gave rise to significant sintering of Au NPs from 2.6 nm to average particle size of 11.1 nm (Fig. S4 in Supporting information). The corresponding energy dispersive spectroscopy (EDS) elemental mapping analysis of the Au/TiO_2@AA-N600 further reveals that Au NPs are homogeneously distributed on the TiO_2 (Fig. 1j), well consistent with the XRD results. Therefore, the above results suggest that the introduction of AA is possible to induce the formation of encapsulation.

Electron energy loss spectra (EELS) examination was performed to identify the composition of the thin overlayer and their chemical states covered on the Au NPs of Au/TiO_2@AA-N600 sample (Fig. 2 and Fig. S5 in Supporting information). It shows that both on the support (region C) and Au NPs surface (region B), Ti L-edge and weak O K-edge signals are observed. Ti signals appearing on the surface of the Au NPs verifiably demonstrated the successful formation of the SMSI overlayer. However, the Ti species in the overlayer were reduced to Ti^{3+} (region B), whereas the Ti species in the supports show a Ti^{4+} signal (region C) (Fig. 2c). These results provide direct evidence that the overlayer is TiO_x ($x < 2$) species coming from the titania support, which is well consistent with previous studies [26]. The strong interaction between metal and support makes the migration of substoichiometric titanium species onto the Au NPs thermodynamically favorable [35]. Besides, as shown in Fig. 2a, an overlayer on Au NPs was observed to form after AA modification and N_2 treatment at 600 °C. These amor-

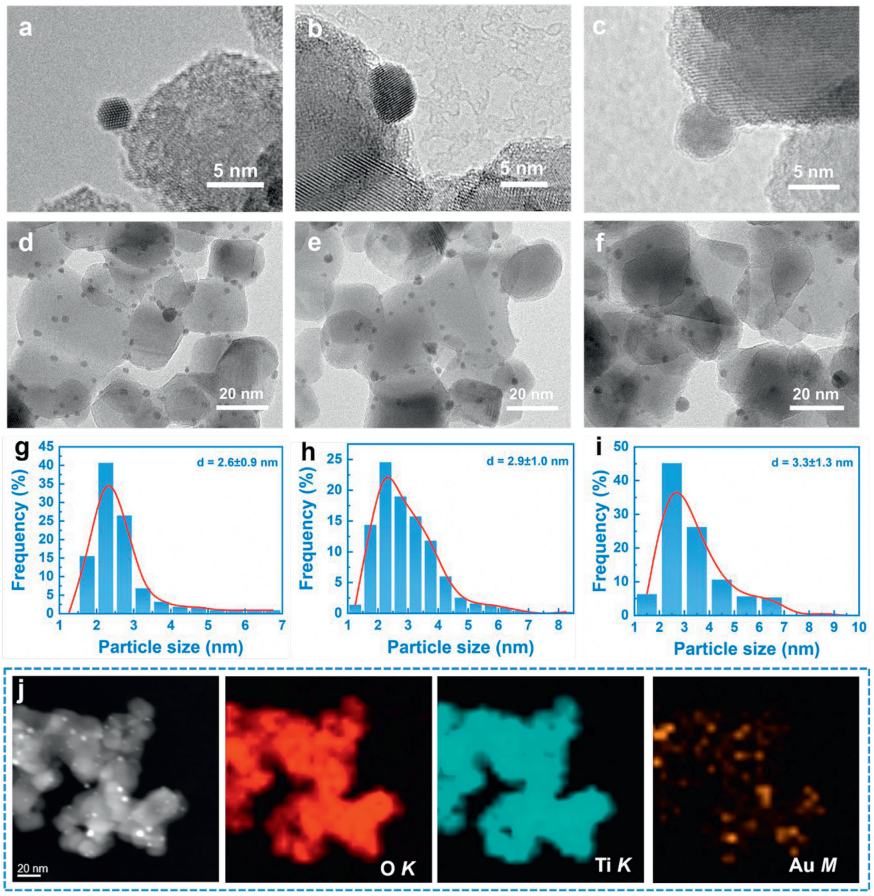

Fig. 1. TEM characterization of the supported Au catalyst. HRTEM, TEM images and the Au particle size distribution of (a, d, g) Au/TiO_2, (b, e, h) Au/TiO_2@AA, and (c, f, i) Au/TiO_2@AA-N600. (j) STEM image and corresponding EDS mapping of O, Ti, and Au elements of the Au/TiO_2@AA-N600 sample.

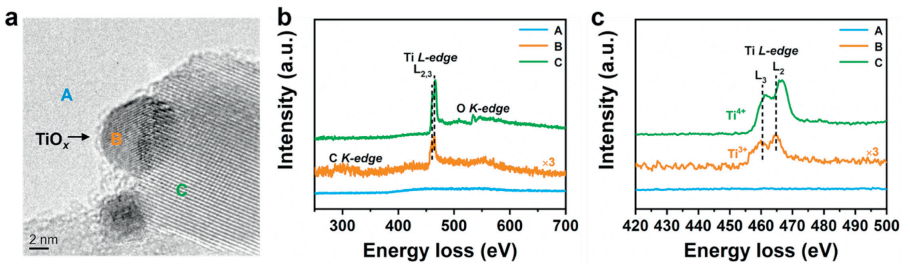

Fig. 2. EELS spectra of Au/TiO_2@AA-N600 catalyst. (a) HRTEM image. (b) EELS spectra characterizing different regions in the image (a) with a range of 250–700 eV. (c) EELS spectra with a range of 420–500 eV in image (b). The spectra were background-subtracted.

phous overlayers are different from the impermeable encapsulation in the classical SMSI, which is a crystalline structure so the reactant molecules cannot contact the active metal [20,24]. Consider our recent finding that the similar permeable overlayers can form through induced by melamine and calcined at 800 °C [26,27], these porous layers maybe keep the metal sites active in a great degree.

Detailed studies were then carried out to unveil the underlying formation mechanism of the encapsulation induced by AA. One of the typical features to verify the SMSI encapsulation of metal NPs is the suppressed CO chemisorption. *In situ* diffuse reflectance infrared Fourier transform spectroscopy (DRIFTS) were measured to study the surface structure and adsorption behavior of Au NPs. As shown in Fig. 3a and Fig. S6 (Supporting information), the Au/TiO_2 sample displays three bands at 2174, 2120, and 2096 cm^{-1}, respectively. The former two peaks are ascribed to gaseous CO and the band at 2096 cm^{-1} is assigned to linear adsorption of CO on metallic Au (CO-Au^0) [36]. After modification with AA, the adsorption of CO on Au NPs almost disappeared, which reflects the limited gold sites. Considering the fact that the size of Au NPs did not change much (from 2.6 nm to 2.9 nm), the decrease of gold sites for CO adsorption could be reasonably assigned to the blockage of Au NPs by the adsorption of AA on their surface rather than the change in the gold dispersion. After helium purging, the very weak signal of linear-bonded CO on the $Au^{\delta+}$ remained and a frequency blue-shift compared with pristine Au/TiO_2 catalyst (from 2096 cm^{-1} to 2126 cm^{-1}) is observed, suggesting the generation of the positively charged $Au^{\delta+}$ species during the AA modification procedure (Fig. S6b in Supporting information). As for Au/TiO_2@AA-N600, even if the gaseous CO peaks are removed by helium purging, the peaks at 2114 cm^{-1} and 2062 cm^{-1} are still observed (Fig. S6c in Supporting information), which are assigned to the linear adsorption of CO on Au^0 and $Au^{\delta-}$ species, respectively [27,34,37–39]. The intensity of CO adsorption decreased drastically in comparison with fresh Au/TiO_2, which can be attributed to the encapsulation at

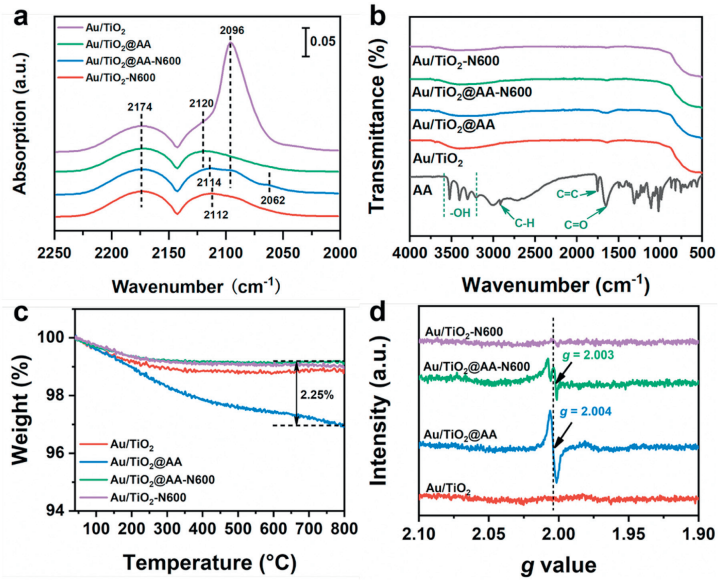

Fig. 3. Mechanism study of AA adsorbate-induced SMSI formation. (a) *In-situ* DRIFT spectra of CO adsorption on various gold catalysts. (b) ATR-IR spectra and (c) TG analysis curve of AA, Au/TiO_2, Au/TiO_2@AA, Au/TiO_2@AA-N600 and Au/TiO_2-N600. (d) EPR spectra of the various Au catalysts at 110 K.

the SMSI state, in good agreement with the HRTRM results (Fig. S3 in Supporting information). More importantly, the CO adsorption is red-shifted relative to that of the uncalcined sample (2126–2114 cm^{-1}) and exhibits a new band around 2062 cm^{-1} (CO-$Au^{\delta-}$), evidencing that surface Au species have a slight negative charge stemmed from electron transfer from support (perhaps the oxygen vacancies) to metal. Despite the existence of the overlayer, the linear CO adsorption signal is still present on Au/TiO_2@AA-N600, which might be due to the existence of gaps/pores on the overlayer supplying channels for CO molecule attaining the gold surface [15,16,20,27,40]. On the other hand, the BET surface area of various catalysts also provides consistent information. Table S2 (Supporting information) displayed that the surface area calculating based on Brunauer–Emmett–Teller (BET) method of Au/TiO_2@AA-N600 is 50.8 m^2/g similar to the unmodified Au/TiO_2 sample (54.8 m^2/g). Comparatively, the BET surface area of Au/TiO_2-N600 catalysts decreased to 44.3 m^2/g, demonstrating that the permeable overlayer is formed after the modification with AA and treatment in N_2 flow [26]. At last, the CO adsorption on 2096 cm^{-1} of Au/TiO_2-N600 totally disappears and only a slight peak at 2112 cm^{-1} (Fig. S6d in Supporting information) is observable, which is ascribed to the CO adsorption on larger Au NPs [34].

One may argue that the presence of carbonaceous species derived from AA deposition on the surface of metal sites, rather than SMSI overlayer, may result in a comparable effect of inhibiting CO chemisorption values [17,41]. To rule out this possibility, the ATR-IR spectra of AA and various Au nanocatalysts were observed, and the four Au-based catalysts do not show pronounced peaks assigned to the adsorbed AA species (Fig. 3b). In addition, the EDS analysis demonstrated that the content of carbon species in the Au catalyst is very low, and a weak amount of signal may come from the organic matter adsorbed on the catalyst surface or the supported carbon film (Fig. S7 in Supporting information). As shown in Fig. 3c, the weight change of the Au catalysts was further investigated by thermogravimetric (TG). It shows only the Au/TiO_2@AA have a 2.25 wt% weight loss, which could be attributed to the complete decomposition of adsorbed AA in the N_2 atmosphere, as evidenced by the decomposition of pure AA starting from 220 °C in N_2 (Fig. S8 in Supporting information). This conclusion can be further verified by a TG measurement in air which shows similar weight loss that originated from the combustion of residual AA (Fig. S9 in Supporting information). Other samples show almost no weight change during the heating process. Accordingly, TG analysis confirms that there is no carbon or carbon-containing organic species present on the surface of Au/TiO_2@AA-N600 catalyst, and the encapsulation on the surface of Au NPs is a TiO_x thin overlayer.

The electronic states of surface elements of the supported Au nanocatalysts were investigated by X-ray photoelectron spectroscopy (XPS). In the Au 4f XPS spectra (Fig. S10a in Supporting information), Au species in the Au/TiO_2 sample are mainly composed of Au^0 with the binding energy (BE) of Au $4f_{5/2}$ at 83.4 eV. However, the binding energy of Au^0 shifting to 83.2 eV can be observed in Au/TiO_2-SMSI sample, indicating that Au NPs exist in an electron-rich state originating from the charge transfer between Au NPs and the support. Compared with Au/TiO_2, the surface atom ratio of Au 4f to Ti 2p of Au/TiO_2@AA-N600 calculated from the XPS spectra decreased significantly (Fig. S11 in Supporting information). This can be ascribed to TiO_x overlayer formation on the Au NPs since the Au content in the bulk catalysts had no significant change (2.4 wt%, ICP results), which is in agreement with EELS results in Fig. 2. However, the reductive Ti^{3+} species were not observed in the Ti 2p XPS spectra of each catalyst (Fig. S10c in Supporting information), which may be due to the too low content of TiO_x species compared with total titanium [21,27].

This A-SMSI which happens upon the adsorption of AA on the surface followed by heat treatment rather than H_2/O_2 treatment at elevated temperatures, is seemingly different from traditional SMSI. However, the driving force behind the formation of A-SMSI has not been clearly understood yet. According to previous literature, the charge transfer between noble metal NPs and supports is a prerequisite to constructing encapsulation over metal NPs [18,42]. In addition, generating a substantial number of oxygen vacancies (O_V) in supports efficiently promotes a disordered surface structure, thus giving rise to the formation of metal oxide overlayers [17,18,43,44]. In this perspective, AA is a natural product with an enediol group containing hydroxyl groups on both sides of the double bond [45]. Owing to the reductive enediol group in the AA structure, its hydrogen atom is more susceptible to dissociation, probably leading to the generated oxygen vacancies in TiO_2, followed by the migration of TiO_x suboxide species to cover the Au NPs. Consequently, electron paramagnetic resonance (EPR) spectra was adopted to study the paramagnetic transition of the oxygen

Table 1
Summary and comparison of different types of SMSIs in Au/TiO_2 catalyst.

Type of SMSI	Occurrence condition	Suppression of adsorption for CO	Electron transfer	Encapsulation layer permeability	Ref.
Classical SMSI	H_2 reduction, 500 °C	Yes	From the support to the metal	No	[24]
Melamine induced SMSI	Melamine induced, pretreated in N_2 (600 °C), followed by calcinated in air (800 °C)	Yes	From the metal to the support	Yes	[27]
AA-induced SMSI	AA-induced, calcined in N_2 (600 °C)	Yes	From the support to the metal	Yes	This work

vacancies at 110 K [46]. As shown in Fig. 3d, no evident EPR response is detected for Au/TiO_2, suggesting its pristine topology has no unpaired electrons. After the AA modification, the distinct EPR signal of Au/TiO_2@AA exhibits at $g = 2.004$, which can be assigned to the unpaired free electrons from O_V and further substantiate introduced AA species resulting in an oxygen-defective structure [47–49]. In parallel, a similar EPR signal of O_V at $g = 2.003$ is also observed for Au/TiO_2@AA-N600 but the intensity of O_V becomes weaker after the heating process. This result points out that O_V helps to activate the surface of the support to form SMSI. Moreover, the O 1s XPS were used to analyze the defective sites of Au catalysts, which contribute to inducing the formation of encapsulation. As shown in Fig. S10b (Supporting information), it can be deconvoluted into three peaks at 529.9, 530.6 and 531.9 eV, which are assigned to the lattice oxygen, oxygen vacancies and other weakly bound oxygen species, respectively [50,51]. The relative ratio of O_V in oxygen species calculated based on the corresponding peak area increased from 7.3% (Au/TiO_2) to 14.9% (Au/TiO_2@AA-N600), in agreement with the EPR results. However, the EPR signal of Au/TiO_2-N600 is negligible, indicating that oxygen vacancies offer an opportunity for the formation of SMSI to stabilize highly active metal NPs. Therefore, the above results notarize the AA-induced the O_V generation and activates the support surface, and then high-temperature treatment promotes support migration to form an SMSI encapsulation structure.

It is notable from the above discussion that the exogenous adsorbent AA, rather than the reaction intermediate, can induce the formation of A-SMSI in the Au/TiO_2 system. This exogenous adsorption method induced A-SMSI is different from the classical SMSI and offers a new horizon for catalyst design and catalytic application. Therefore, it is worth summarizing and comparing the characteristics of various types of SMSI in the Au/TiO_2 system (Table 1) to further understand and explore the SMSI phenomenon. For classical SMSI, abundant TiO_x overlayers migrated onto the surface of Au NPs to form crystalline encapsulation structures after high-temperature reduction [24]. The electron transfer, suppression of small-molecule adsorption, and reversible metal encapsulation were consistent with the Pt/TiO_2 system. However, this SMSI always lead to deterioration of reaction activity by covering active sites for activation of reactants. Our reported exogenous adsorption strategy, induced by AA, exhibits electronic interaction between Au and TiO_2, and suppression of CO adsorption, which are similar to those of the classical SMSI. On the other hand, this permeable overlayer enables access for the reactants to interact with the active sites, thus the Au/TiO_2 catalysts with A-SMSI can exhibit excellent activity and sintering resistance. These differences also demonstrate that different strategies induce SMSI through different mechanisms. Therefore, exogenous adsorption methods to construct A-SMSI with porous overlayers are new ways to harness SMSI and catalyst design.

CO oxidation as an important model reaction at lab-scale conditions was chosen to investigate the catalytic performance of a series of Au catalysts because of its importance in both fundamental studies and practical applications [52]. In particular, it is a structure-sensitive reaction and its catalytic behavior is highly dependent on the size of metal NPs. As shown in Fig. 4a, Au/TiO_2 exhibits remarkable catalytic activity and achieves complete conversion of CO at ambient temperature. Obviously, Au/TiO_2@AA-N600 exhibits outstanding catalytic performance with complete CO conversion at 20 °C even after the high-temperature treatment. Based on the above HRTEM results, this surprising activity can be ascribed to the permeable encapsulation of gold by the TiO_x overlayer. This encapsulation inhibits the sintering of Au NPs while allowing the reactant molecules to the gold site's surface. However, the Au/TiO_2@AA catalyst exhibited a noticeable decrease in activity after AA modification, which is probably linked to AA blocks metal active sites, in good agreement with the DRIFT results (Fig. 3a). In contrast, the catalytic activity of the Au/TiO_2-N600 catalyst was dramatically decreased after treated at 600 °C in N_2 flow and the value of T_{50} increases to 110 °C. Combined with the TEM characterization results, the inferior activity might be attributed to the noticeable sintering of the Au NPs with a larger mean Au size of 11.1 nm (Fig. S4 in Supporting information). To compare the intrinsic activity of catalysts, the specific rate of the above catalysts and the corresponding turnover frequency (TOF) at 25 °C were measured at the kinetic region and calculated, respectively. As shown in Fig. 4b and Table S3 (Supporting information), it confirmed the reaction-specific rate and TOF value of Au/TiO_2 are 1.42 $mol_{CO}\ g_{Au}^{-1}\ h^{-1}$ and 0.22 s^{-1}, respectively, similar to the previous studies [27,53,54]. Regarding Au/TiO_2@AA-N600, the reaction rate and TOF decrease to 0.14 $mol_{CO}\ g_{Au}^{-1}\ h^{-1}$ and 0.03 s^{-1}. Although they are lower than that of the fresh Au/TiO_2 catalysts, they also rival other sintering-resisted Au-based catalysts reported in the literature (Table S3). Correspondingly, the Au/TiO_2-N600 catalysts with obvious sintering brought about a dramatically decreased reaction rate of about 47-fold from 1.42 $mol_{CO}\ g_{Au}^{-1}\ h^{-1}$ to 0.03 $mol_{CO}\ g_{Au}^{-1}\ h^{-1}$.

The above results have shown that the overlayer on the Au/TiO_2@AA-N600 sample can stabilize the gold NPs against sintering, implying a potentially good catalytic stability of the catalyst during the reaction. In practical application processes such as auto-exhaust elimination, the catalyst will face repeated cold-hot cycling. Thus, the cycle performance of this catalyst was investigated (Fig. 4c). It turns out that during successive six cycles running up to 600 °C, the catalyst activity remains unchanged, indicating that this catalyst holds promising repeating start-up performance for practical applications. On the contrary, a significant loss of activity immediately occurred for Au/TiO_2 in the second test (Fig. S12 in Supporting information), most probably due to the sintering of Au NPs on this catalyst [23]. The long-term stability was further evaluated at 300 °C with a higher gas hourly space velocity (GHSV = 1371 $L\ g_{cat.}^{-1}\ h^{-1}$). As shown in Fig. 4d, there is no significant deactivation in a 50-h continuous test, further confirming its good sintering resistance. Of more interest, we also tested the sample at 30 °C where the accumulation of CO_2 is a common performance [55]. It shows that the conversion remains nearly constant over 100 h (Fig. S13 in Supporting information), indicating that our samples even have good resistance to CO_2 accumulation. All these results demonstrated that the TiO_x overlayers on the Au NPs after SMSI construction provide excellent activity and stability.

To evaluate the universality of SMSI construction induced by AA adsorption and high-temperature treatment, a series of sup-

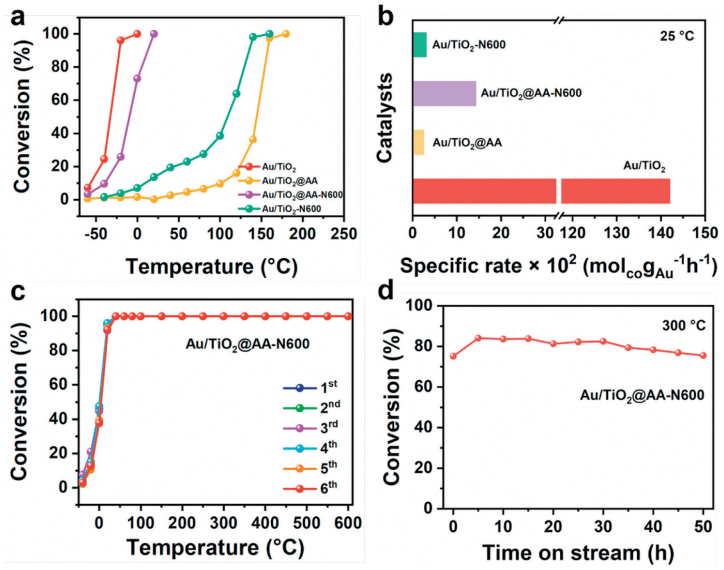

Fig. 4. Catalytic performance of the Au nanocatalysts in CO oxidation. (a) CO conversion as a function of reaction temperature with a feed gas comprising 1 vol% CO, 1 vol% O_2 and 98 vol% He at 33.3 mL/min. (b) Corresponding specific reaction rate for different Au catalysts with CO oxidation at 25 °C. (c) Conversion of CO from −40 °C to 600 °C with six cycles of testing on Au/TiO_2@AA-N600 catalyst. (d) CO conversion as a function of reaction time at 300 °C on Au/TiO_2@AA-N600 catalyst with space velocity of 1371 L $g_{cat.}^{-1}$ h^{-1}.

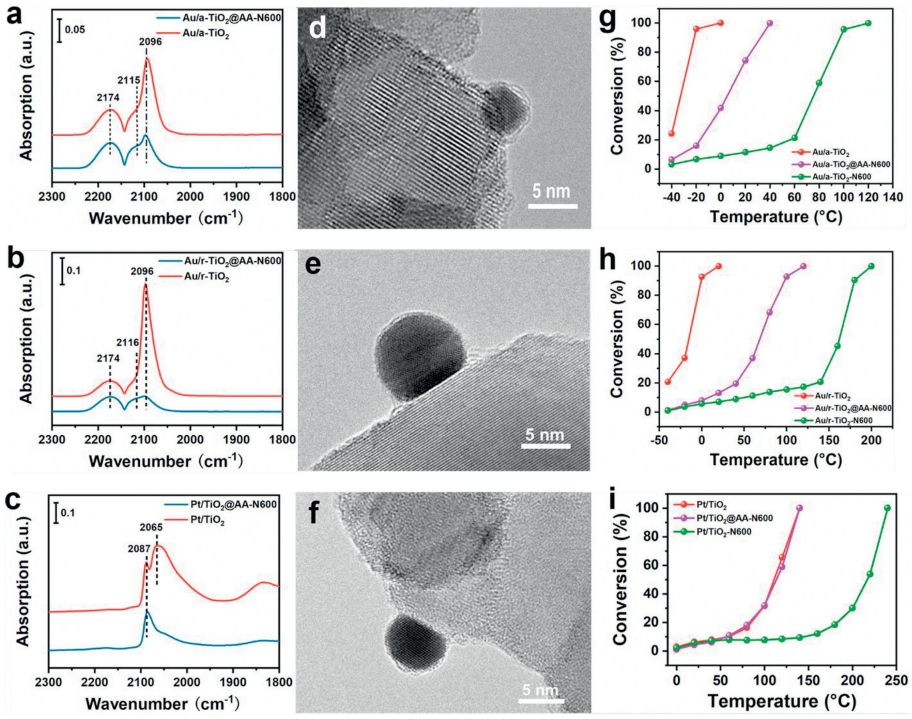

Fig. 5. Characterization and CO oxidation performance of AA-induced SMSI catalysts. (a–c) *In-situ* DRIFT spectra of CO adsorption and HRTEM images of (d) Au/a-TiO_2@AA-N600, (e) Au/r-TiO_2@AA-N600, and (f) Pt/TiO_2@AA-N600 nanocatalysts after AA and high-temperature treatment under N_2 atmosphere at 600 °C. (g–i) Catalytic performance of different catalysts in the CO oxidation reaction. Reaction conditions: reaction gas comprising 1 vol% CO, 1 vol% O_2, and 98 vol% He, gas flow rate of 33.3 mL/min.

ported noble metal catalysts were synthesized. To investigate the effect of the support crystal phase, the AA-induced SMSI was studied on anatase and rutile TiO_2-supported Au NPs. It can be observed all the Au/TiO_2-SMSI catalysts possess encapsulated Au NPs, as evidenced by DRIFT results (Figs. 5a and b, Figs. S14 and S16 in Supporting information) and HRTEM (Figs. 5d and e, Figs. S15 and S17 in Supporting information). Consistently, the Au/a/r-TiO_2@AA-N600 samples with SMSI have shown slightly decreased activity compared with the pristine Au/a/r-TiO_2 but still much better than Au/a/r-TiO_2-N600 samples (Figs. 5g and h). Furthermore, a series of TiO_2 (P25) supported PGM catalysts (*e.g.*, Pt, Pd, and Rh) were also prepared and modified by AA. A detailed study in combination with DRIFT and HRTEM suggests that in analogy to the Au/TiO_2-AA-induced SMSI case, all samples displayed diminished CO chemisorption (Fig. 5c, Figs. S18, S20, and S21 in Supporting information), indicating that the group VIII metals Pt, Pd, and Rh can have similar overlayers encapsulating the metal NPs, as evidenced by HRTEM images (Fig. 5f and Fig. S19 in Supporting information). Catalytic performance test reveals that AA modification can maintain better reactivity compared to the coun-

terpart sample without AA treatment only a high-temperature process (Fig. 5i).

As shown in Figs. S22 and S23 (Supporting information), encapsulation did not occur when treatment in N_2 atmosphere at lower temperatures (400 °C and 500 °C), indicate treatment temperature at 600 °C is requisite to make the SMSI happen. The catalytic test for CO oxidation was conducted to compare the performance of Au catalysts treated at different temperatures (Fig. S24 in Supporting information). There is a significant enhancement in CO conversion when the temperature is increased to 300 °C. Combined with the TG results (Fig. S8), this enhancement of activity can attribute to the decomposition of AA adsorbed on the surface of Au particles at 300 °C makes the active sites accessible. As the temperature increases to 400 °C and 500 °C, the catalytic activity further increases while slight decrease when the treatment temperature increases to 600 °C. The slight decrease might be related to the occurrence of the SMSI. This result corroborating the 600 °C treatment in N_2 is necessary. Furthermore, the Au/TiO_2@AA catalysts treated by high-temperature (600 °C) under different atmosphere (Ar/He) to demonstrate the influence of atmosphere on SMSI phenomenon. The catalysts were denoted as Au/TiO_2@AA-Ar600 and Au/TiO_2@AA-He600, respectively. As shown in Figs. S25 and S26 (Supporting information), TEM results of Au catalysts under different atmosphere treatment show Au NPs are well dispersed on TiO_2 support, in which the mean particle size of Au was ~3.5 nm and ~3.3 nm, respectively, similar with the Au samples treatment under N_2 atmosphere (Fig. 1i). From the HRTEM images, the Au NPs can also be encapsulated by TiO_x overlayer, consistent with the results of Au/TiO_2@AA-N600 in the Fig. 1. In addition, the CO-DRIFTS experiments on various Au samples exhibited a decrease in intensity for both Au/TiO_2@AA-Ar600 and Au/TiO_2@AA-He600 sample (Fig. S27 in Supporting information), which can be ascribed to the loss of CO adsorption sites resulting from the encapsulation of Au NPs by TiO_x, consistent with HRTEM results. Therefore, an inert atmosphere might be necessary for SMSI formation but N_2 is not indispensable. All above results validate the widespread applicability of this AA adsorption-induction strategy.

In summary, for the first time, we have found that the A-SMSI between Au NPs and TiO_2 support can be constructed by L-ascorbic acid adsorption and induction, followed high-temperature treatment at 600 °C under an inert atmosphere. The unique approach forms permeable TiO_x thin overlayers on the Au NP surface, thus the Au/TiO_2 catalysts with this SMSI can exhibit excellent activity and sintering resistance. The presence of the reductive enediol group in the AA is essential for promoting the generation of the oxygen vacancies on the support, which is a prerequisite for activating the surface of the support. High temperature treatment drives the migration of partially reduced support derivatives to form encapsulated structures. Of more importance, this strategy is general and can be extended to other noble metal catalysts, providing new insight into activating the support surface and constructing SMSI, thus paving a horizon for designing the encapsulated metal NPs catalysts and modulating the catalytic performance.

Declaration of competing interest

The authors declare that they have no known competing financial interests or personal relationships that could have appeared to influence the work reported in this paper.

CRediT authorship contribution statement

Yunxia Liu: Writing – original draft, Visualization, Methodology, Investigation, Conceptualization. **Guandong Wu:** Formal analysis. **Lin Li:** Resources, Formal analysis. **Yiming Niu:** Visualization, Investigation. **Bingsen Zhang:** Resources, Formal analysis. **Botao Qiao:** Writing – review & editing, Supervision, Funding acquisition. **Junhu Wang:** Writing – review & editing, Supervision, Funding acquisition.

Acknowledgments

This work was supported by the National Natural Science Foundation of China (NSFC) and the Japan Society for the Promotion of Science (JSPS) under the Joint Research Program (Nos. NSFC21961142006 and JPJSJRP20191804) as well as the NSFC (Nos. U22A20394 and 22375200), the DICP.CAS-Cardiff Joint Research Units (No. 121421ZYLH20230008) and the International Partnership Program of Chinese Academy of Sciences (No. 028GJHZ2023097GC). G. Wu is grateful to the China Postdoctoral Science Foundation (No. 2022M723086).

Supplementary materials

Supplementary material associated with this article can be found, in the online version, at doi:10.1016/j.cclet.2024.110608.

References

[1] W.T. Grubb, D.W. Mckee, Nature 210 (1966) 192–194.
[2] A. Beck, X. Huang, L. Artiglia, et al., Nat. Commun. 11 (2020) 3220.
[3] S. Mitchell, R. Qin, N. Zheng, J. Pérez-Ramírez, Nat. Nanotechnol. 16 (2020) 129–139.
[4] Q. Zhang, X.X. Qin, F.P. Duan-Mu, et al., Angew. Chem. Int. Ed. 57 (2018) 9351–9356.
[5] Y. Luo, D. Wang, Acta Phys. Chim. Sin. 39 (2023) 2212020.
[6] S. Peng, Y. Rao, T. Li, et al., Chin. Chem. Lett. 35 (2024) 109219.
[7] S.J. Tauster, S.C. Fung, R.L. Garten, J. Am. Chem. Soc. 100 (1978) 170–175.
[8] S.J. Tauster, Acc. Chem. Res. 20 (1987) 389–394.
[9] M. Xu, S. Yao, D. Rao, et al., J. Am. Chem. Soc. 140 (2018) 11241–11251.
[10] T.W. van Deelen, C. Hernández Mejía, K.P. de Jong, Nat. Catal. 2 (2019) 955–970.
[11] T. Pu, W. Zhang, M. Zhu, Angew. Chem. Int. Ed. 62 (2022) e202212278.
[12] S.J. Tauster, S.C. Fung, R.T.K. Baker, J.A. Horsley, Science 211 (1981) 1121–1125.
[13] F. Zhang, H. Guo, M.H. Liu, et al., Chin. J. Catal. 48 (2023) 195–204.
[14] Q. Zhang, X. Jiang, Y. Su, Y. Zhao, B. Qiao, Chin. J. Catal. 57 (2024) 105–113.
[15] J. Zhang, H. Wang, L. Wang, et al., J. Am. Chem. Soc. 141 (2019) 2975–2983.
[16] J. Zhang, D. Zhu, J. Yan, C.A. Wang, Nat. Commun. 12 (2021) 6665.
[17] K.M. Siniard, M. Li, S.Z. Yang, et al., Angew. Chem. Int. Ed. 62 (2023) e202214322.
[18] M. Li, T. Zhang, S.Z. Yang, et al., ACS Catal. 13 (2023) 6114–6125.
[19] J. Zhang, J. Ma, T.S. Choksi, et al., J. Am. Chem. Soc. 144 (2022) 2255–2263.
[20] J.C. Matsubu, S. Zhang, L. DeRita, et al., Nat. Chem. 9 (2017) 120–127.
[21] Q. Fu, T. Wagner, S. Olliges, H.D. Carstanjen, J. Phys. Chem. B 109 (2005) 944–951.
[22] R. Meyer, C. Lemire, S.K. Shaikhutdinov, H.J. Freund, Gold Bull. 37 (2004) 72–124.
[23] D.W. Goodman, Catal. Lett. 99 (2005) 1–4.
[24] H. Tang, Y. Su, B. Zhang, et al., Sci. Adv. 3 (2017) e1700231.
[25] F. Hong, S. Wang, J. Zhang, et al., Chin. J. Catal. 42 (2021) 1530–1537.
[26] S. Liu, H. Qi, J. Zhou, et al., ACS Catal. 11 (2021) 6081–6090.
[27] S. Liu, W. Xu, Y. Niu, et al., Nat. Commun. 10 (2019) 5790.
[28] J. Long, X. Zheng, B. Wang, et al., Chin. Chem. Lett. 35 (2024) 109354.
[29] S. Zhang, P.N. Plessow, J.J. Willis, et al., Nano Lett. 16 (2016) 4528–4534.
[30] S.J. Tauster, S.C. Fung, J. Catal. 55 (1978) 29–35.
[31] G.J. den Otter, F.M. Dautzenberg, J. Catal. 53 (1978) 116–125.
[32] H. Tang, J. Wei, F. Liu, et al., J. Am. Chem. Soc. 138 (2016) 56–59.
[33] K. Zhao, H. Tang, B. Qiao, L. Li, J. Wang, ACS Catal. 5 (2015) 3528–3539.
[34] H. Wang, L. Wang, D. Lin, et al., Nat. Catal. 4 (2021) 418–424.
[35] S. Sakellson, M. McMillan, G.L. Haller, J. Phys. Chem. 90 (1986) 1733–1736.
[36] I.X. Green, W. Tang, M. Neurock, J.T. Yates Jr., Science 333 (2011) 736–739.
[37] X. Liu, M.H. Liu, Y.C. Luo, et al., J. Am. Chem. Soc. 134 (2012) 10251–10258.
[38] X. Du, Y. Huang, X. Pan, et al., Nat. Commun. 11 (2020) 5811.
[39] Y. Zhang, J.X. Liu, K. Qian, et al., Angew. Chem. Int. Ed. 60 (2021) 12074–12081.
[40] Y. Gangarajula, F. Hong, Q. Li, et al., Appl. Catal. B 343 (2024) 123503.
[41] F. Polo-Garzon, T.F. Blum, V. Fung, et al., ACS Catal. 10 (2020) 8515–8523.
[42] Y. Li, Y. Zhang, K. Qian, W. Huang, ACS Catal. 12 (2022) 1268–1287.
[43] P. Wu, S. Tan, J. Moon, et al., Nat. Commun. 11 (2020) 3042.
[44] Y. Zhang, W. Yan, H. Qi, et al., ACS Catal. 12 (2022) 1697–1705.
[45] M. Axelsson, C.F.N. Marchiori, P. Huang, C.M. Araujo, H. Tian, J. Am. Chem. Soc. 143 (2021) 21229–21233.
[46] Z.V. Saponjic, N.M. Dimitrijevic, O.G. Poluektov, et al., J. Phys. Chem. B 110 (2006) 25441–25450.
[47] L. Luo, X. Han, K. Wang, et al., Nat. Commun. 14 (2023) 2690.
[48] T. Wei, S. Zhang, Q. Liu, et al., Acta Phys. Chim. Sin. 39 (2023) 2207026.
[49] Y. Zhang, Y. Liu, W. Guan, et al., Chin. Chem. Lett. 35 (2024) 108932.

[50] X. Chen, L. Liu, P.Y. Yu, S.S. Mao, Science 331 (2011) 746–750.
[51] B. Safavinia, Y. Wang, C. Jiang, et al., ACS Catal. 10 (2020) 4070–4079.
[52] H.J. Freund, G. Meijer, M. Scheffler, R. Schlogl, M. Wolf, Angew. Chem. Int. Ed. 50 (2011) 10064–10094.
[53] Y. Zhang, J. Zhang, B. Zhang, et al., Nat. Commun. 11 (2020) 558.
[54] H. Tang, F. Liu, J. Wei, et al., Angew. Chem. Int. Ed. 55 (2016) 10606–10611.
[55] K. Zhao, B. Qiao, Y. Zhang, J. Wang, Chin. J. Catal. 34 (2013) 1386–1394.